Effect of additive manufacturing process parameters on the titanium alloy microstructure, properties and surface integrity

Seyyed-Saeid Biriaie, Mohammed Nouari, Houssemeddine Ben Boubaker, Pascal Laheurte

Available online at www.sciencedirect.com

ScienceDirect

Procedia CIRP 00 (2022) 000–000

www.elsevier.com/locate/procedia

6th CIRP Conference on Surface Integrity

Effect of additive manufacturing process parameters on the titanium alloy microstructure, properties and surface integrity

Seyyed-Saeid Biriaie[a], Mohammed Nouari[a,*], Houssemeddine Ben Boubaker[a], Pascal Laheurte[b]

[a]*LEM3, UMR-CNRS 7239, Université de Lorraine, IMT-GIP-InSIC, 27 rue d'Hellieule, F88100, St-Dié-des-Vosges, France*
[b]*LEM3, UMR-CNRS 7239, Université de Lorraine, Arts et Métiers Institute of Technology, 7, rue Félix Savart, 57070, Metz, France*

* Corresponding author. Tel.: +33-329-422-226; fax: +33-294-218-825. *E-mail address:* mohammed.nouari@univ-lorraine.fr

Abstract

Damage initiation and propagation are widely impacted by pores distribution induced during additive manufacturing (AM) processes. More specifically, the porosity can strongly affect the thermomechanical behavior of titanium alloys in the case of Selective Laser Melting (SLM). The present work examined the impact of SLM process parameters on microstructure characteristics, mechanical properties, and surface integrity of the Ti6Al4V titanium alloy. Different metallographic analyses (i.e., Scanning Electron Microscopy (SEM), and X-Ray Diffraction (XRD)), density measurement and surface characterizing were carried out to investigate the effect of various process parameters (laser power and scanning speed) on the damage behaviors in terms of fracture surface and cracks initiation sites of the alloy.

Keywords: Additive Manufacturing; SLM; Microstructure; Mechanical Properties; Surface Integrity

1. Introduction

Nomenclature

AM	Additive Manufacturing
PBF	Powder Bed Fusion
SLS/SLM	Selective Laser Sintering/Melting
EBM	Electron Beam Melting

Additive manufacturing (AM), also known as 3d printing, has raised lots of attention both in academic fields and industries. This manufacturing process, in which each part is formed layer by layer, consists of multiple techniques and since today it has been employed for different materials (metallic, polymer, …). This variety of techniques and the possibility of using a wide range of materials make this method widely used in the aeronautics, automotive, and medical industries [1]. The premier works on producing additively manufactured parts have been started by introducing the rapid prototyping process in 1980; since then, 3d printing technology has constantly been evolving, and new processes are being explored and presented [2].

The recent developments in the field of additive manufacturing led to the manufacturing of segments made of the so-called difficult-to-machine metals, such as titanium alloys and nickel-based super-alloys. In latest years, powder form of metals such as Titanium (Ti6Al4V [3, 4], TiNb [5, 6],…), (Stainless steel 316L [7], Maraging steel 18Ni 300 [8], …), Nickel-based super-alloys (Inconel 625 [9], Inconel 718 [10], …), have been used by powder bed fusion (PBF) processes such as Selective Laser Sintering (SLS), Selective Laser Melting (SLM), and Electron Beam Melting (EBM).

The advantages of metal additive manufacturing, such as design freedom, the possibility of fabricating complex geometries, and shorter fabrication time compared to the conventional manufacturing methods, along with impressive capabilities of Ti6Al4V titanium alloys such as

biocompatibility, excellent corrosion resistance, and low density, had led to the greater attention from industries, aeronautics, and biomedical applications. [11–13]. Despite these enormous benefits of fabricating these alloys with additive manufacturing methods, the mechanical properties and surface integrity of as-printed components raised concerns about its use more than before. These mechanical characteristics are highly dependent on the 3d printing process parameters, such as laser power, scanning speed, layer thickness, and hatch spacing [14–17].

Also, surface integrity is a crucial parameter in the evaluation of the AM components quality. Due to the layer-wise procedure of manufacturing parts with the additive manufacturing process, the finished surface of the parts is drastically affected, and post-processing methods, such as machining, are essential [18–21].

Finally, the additive manufacturing process parameters, the differences in powders size and powder-to-laser absorptivity, lead to some limitations for obtaining a homogeneous as-build microstructure of Ti6Al4V titanium alloys. The as-build microstructures generally show undissolved particles and porosities. As a result, for example, the machinability of this alloy, which is considered as a difficult-to-machine metal, becomes more complicated since the development of the material damage during machining is widely impacted by the pore distribution induced during additive manufacturing processes.

Regarding the literature, the laser power and scanning speed relate a preeminent role in the mechanical properties and surface integrity of additively manufactured parts, so the main objective of this work is to study the effect of these two process parameters on the microstructure, micro-hardness, and roughness of the as-SLMed Ti6Al4V titanium samples.

2. Experimental Procedure

2.1. Microstructure

The material used for this study is a gas-atomized spherical Ti-6Al-4V grade 23 Titanium powder with a particle size of 28 µm (D10), 38 µm (D50), and 50 µm (D90). The theoretical density of Ti-6Al-4V Titanium is 4.43 g/cm^3, and according to the datasheet of the powder supplier the chemical composition is reported in Table 1.

Table 1. Chemical composition (in wt %) of Ti-6Al-4V Titanium powder.

Chemical composition (wt. %)							
Al	V	C	Fe	O	N	H	Ti
6.26	4.07	<0.01	<0.2	<0.1	<0.01	<0.002	Balance

2.2. Sample fabrication

The SLM samples are fabricated using a SLM 280 HL (SLM Solutions) machine under an inert atmosphere of argon. Many different parameters can affect the additively manufactured components' microstructure and mechanical properties, such as laser power, scanning speed, hatch spacing, layer thickness, etc. These different process parameters are considered through an important factor, energy density (Ev or E, J/mm^3) which is described as the average applied energy per volume of material during a PBF process. The energy density of an additively manufactured sample is expressed according to *Eq (1)*, where *P* is the laser power (W), *v* is the scanning speed (mm/s), h is the hatch spacing (µm), and *t* is the layer thickness (µm).

$$E = \frac{P}{vht} \quad (1)$$

In order to minimize and prioritize the effect of process parameters on the final properties of the SLMed samples, all the process parameters are kept constant except the laser power and scanning speed (layer thickness: 30 µm, hatch spacing: 80 µm, powder bed pre-heated to 200 °C, spot size: 60 µm, pattern type, and rotation: Meander 67°). The different configurations of laser power (125, 150, and 175 W), and scanning speed (375, 550, and 725 mm/s) are selected for this study. To analyze the effect of laser power and scanning speed on the microstructure and mechanical properties of SLMed components, five different conditions are fabricated based on the energy densities of 166.7, 132.6, 113.6, 94.7, and 86.2 J/mm^3. In this regard, the laser power of 150 W keeps constant to fabricate samples with selected scanning speed, and then the scanning speed of 550 mm/s is fixed to manufacture samples with the selected laser power. The configuration of the 3d printing process parameters and energy densities of samples are summarized in Table 2.

Table 2. The configuration of the 3d printing process parameters and energy densities of samples.

Power (W) / Scan Speed (mm/s)	**175**	**150**	**125**
375		166.7	
550	132.6	113.6	94.7
725		86.2	

The cubic samples (10×10×10 mm^3) are used for the SEM observation, XRD measurements, and density measurements. Also, the 3d-printed blocks with the dimension of 130×95×4 mm^3 are used for the roughness test. These blocks are cut into the desired dimension of the tensile specimens for future studies on the mechanical properties.

2.3. Observation and density measurement

The microstructure of the Ti6Al4V samples is observed using the Scanning Electron Microscope JOEL 6100. The cubic samples are cut perpendicular to the building direction, then polish up to 2000 by sandpaper following by etching in Kroll's reagent (100 ml of H2O, 2.5 ml of HNO3, 1.5 ml of HCl, and 1.0 ml of HF) for the microstructure observation. Then, the

X-ray diffractometer analysis were performed on this samples using D8 Advance Bruker XRD machine.

Considering Archimedes' principle according to ASTM B311-17, density measurements are performed by measuring the 3d-printed cubic samples. The Precisa XB 220A hydrostatic weighing system equipped with a wire basket support arrangement as described in ASTM B311-17 is used for the density measurements. Each specimen is weighed up to 5 times both in the air (M_{Air}) and then in the demineralized water (M_{Fluid}). After the measurement of the sample in demineralized water, the wire basket support arrangement is weighed in the same depth of the water as before (M_{Wire}). The measured density of each sample (ρ_{Sample}) could be obtained according to Eq (2); by considering the density of the demineralized water (ρ_{Fluid}, at a specific temperature of the fluid during the measurement). The Amprobe TMD-56 Multi-logging Digital Thermometer with an accuracy of 0.1 °C used to measure the temperature of the water. To prevent the trapping of demineralized water in the pores between each measurement, further surface cleaning and drying for each sample are taken into account. Then, the measured density of additively manufactured samples is compared to the theoretical density of the Ti-6Al-4V material to calculate the porosity according to Eq (3).

$$\rho_{Sample} = \frac{M_{Air} * \rho_{Fluid}}{(M_{Air} - M_{Fluid} + M_{Wire})} \quad (2)$$

$$\%Porosity = 100 - \left(\frac{\rho_{Sample} * 100}{\rho_{Theoretical}}\right) \quad (3)$$

2.4. Hardness test

The Vickers micro-hardness (HV) is measured using the ZWICK ZHV1 Micro-hardness Tester for the cubic samples, with a load of 2.94 N (300 g) and a dwell time of 10 s. For the reliability of the micro-hardness data, up to 20 points are randomly chosen on each 3d printing condition.

2.5. Surface characterization

The Bruker® 3D interferometer is used to obtain the surface roughness and 3d mapping of the 3d-printed blocks; it allows two-dimensional and three-dimensional measurements on surfaces with a precise resolution (<0.1 nm). Up to 8 measurements are performed for each 3d printing condition (1 mm^2 of the surface area is taken for each measurement).

3. Results and discussion

3.1. Microstructure

The SEM observations of the 3d printing samples according to the configuration of additive manufacturing process parameters represented in Table 2 are shown in Fig 1 (the cross sectional surface perpendicular to the building direction). The pictures in each row represented the samples fabricated with the same scanning speed but the different laser power values (with decreasing order from left to right). This configuration was altered for the pictures in each column which showed the 3d-printed samples with the same laser power but the different values of scanning speed (with increasing order from top to bottom). As shown in Fig 1, for the samples fabricated with the lowest scanning speed, which increased the energy density regarding *Eq (1)*, the size and ratio of the porosities is much higher than the highest scanning speed. In addition, the size and ratio of porosities vary from higher laser power values (left to right) in each row.

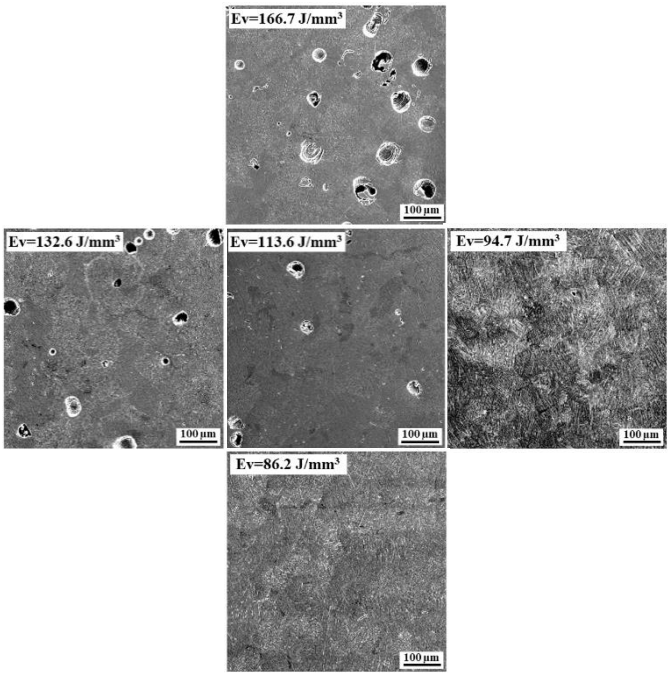

Fig 1. SEM observations of the 3d printing samples with the configuration of AM process parameters shown in Table 2.

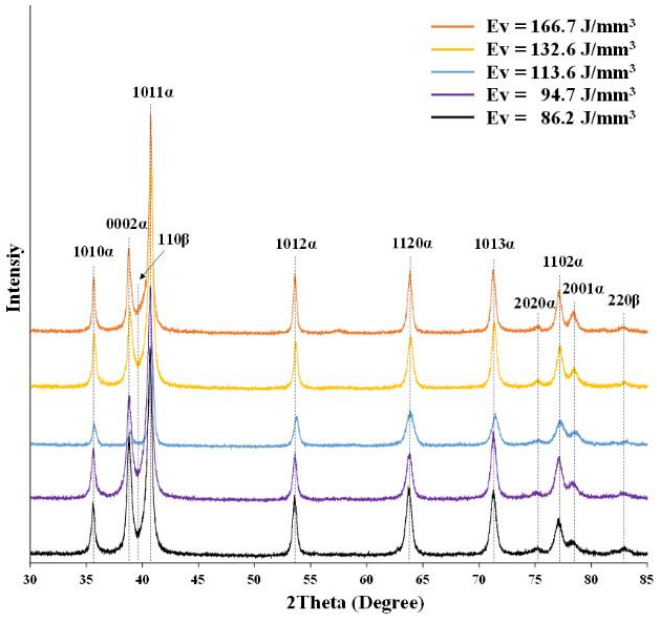

Fig 2. XRD patterns of the additively manufactured Ti-6Al-4V samples for all conditions.

It could be figured out that by decreasing the values of energy density from 166.7 J/mm^3 to 86.2 J/mm^3 (due to the increase of scanning speed value), and also from 132.6 J/mm^3 to 94.7 J/mm^3 (due to the decreasing of laser power value), it is more favorable to obtain the microstructure with minor manufacturing defects in lower energy densities.

The XRD patterns of the additively manufactured Ti-6Al-4V samples for all conditions are shown in Fig 2. XRD patterns of as-SLMed microstructures are composed of the respective peaks of BCC β and HCP α' phases. To better understand the effect of the AM process parameters on the 3d-printed samples and the microstructure and porosity formation, the surface had been cut into three perpendicular planes (see Fig 3. a). The SEM observation of the different planes for the fabricated samples of 113.6 J/mm^3 (Fig 3. b-d) showed the homogeneities in the microstructure of the alloy, and the size of the porosity did not change with regards to the building direction of printing.

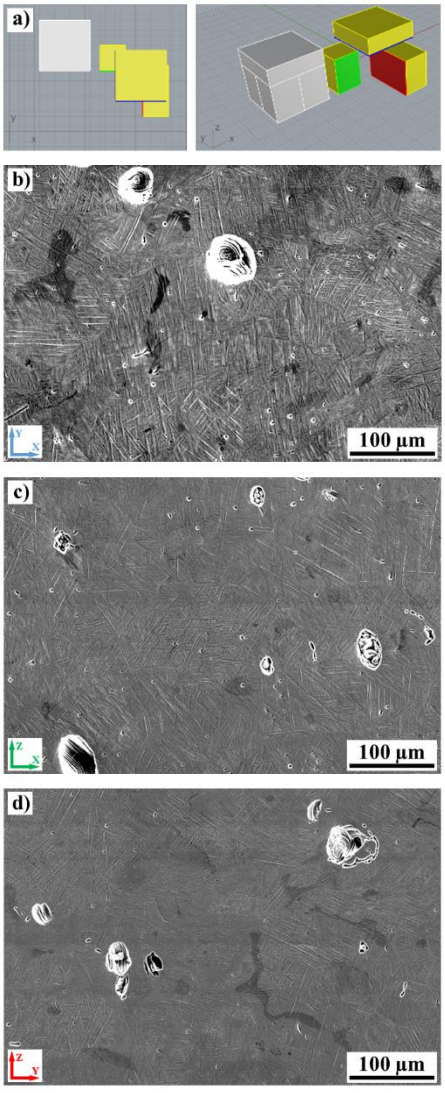

Fig 3. a) 3D-printed cubic sample cut into three perpendicular planes; and the SEM observation of the different planes for the sample of Ev = 113.6 J/mm^3: b) Perpendicular to build direction, plane y-x, c) Parallel to build direction, plane z-x, d) Parallel to build direction, plane z-y.

3.2. Density measurements

The porosity measured by Archimedes' method with respect to the energy density of samples in increasing order is shown in Fig 4. The results showed that the higher energy density value increased the porosity percentage during the manufacturing process. Higher energy densities implied more internal defects in the samples, whether increasing the laser power or lowering the scanning speed. These internal defects increased the porosities level, which negatively affected the mechanical properties of the 3d-printed components. Regards to the porosity measurements, the fabricated samples with energy densities of 86.2 J/mm^3 showed the lowest porosity ratio, which is more favorable for additively manufactured components. As noted in Table 1, for the samples in the column (Power equal to 150 W) the energy density decreased from 166.7 to 86.2 J/mm^3, the porosity results for these samples showed a significant decrease from 5.3 to 0.5%. But the samples in the row (Scanning speed equal to 550 mm/s) showed the slighter decrease as the energy density decrease. The porosity results for the SLMed Ti-6Al-4V reported by Kasperovich et al. [16] and Gong et al. [17] showed similar trend as discussed.

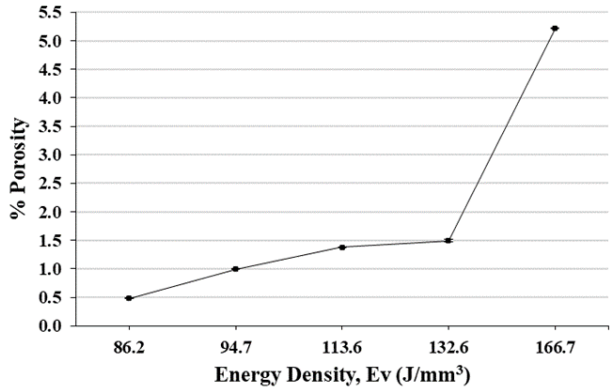

Fig 4. Porosity measurements with respect to the energy.

3.3. Micro-Hardness results

To understand the effect of the different process parameters on the hardness of the additively manufactured samples, the Vickers micro-hardness (HV) had been performed on the top surface (perpendicular to the building direction) of 3d-printed cubic samples, and the micro-hardness results as a function of energy density is presented in Fig 5. The results showed that as the energy density of the printed samples decreases, the hardness of the sample will also decrease slightly but this change is not tangible. The micro-hardness results varied from 385±5 HV. It can be noted that the similar results are reported by Nikiel et al [22] and Benedetti et al. [23] with the average microhardness results for the as-SLMed Ti-6Al-4V grade 23 of 387±9 HV and 380±10 HV, respectively. As the microstructure did not change during the manufacturing process despite the change in the energy density, this behavior was predictable.

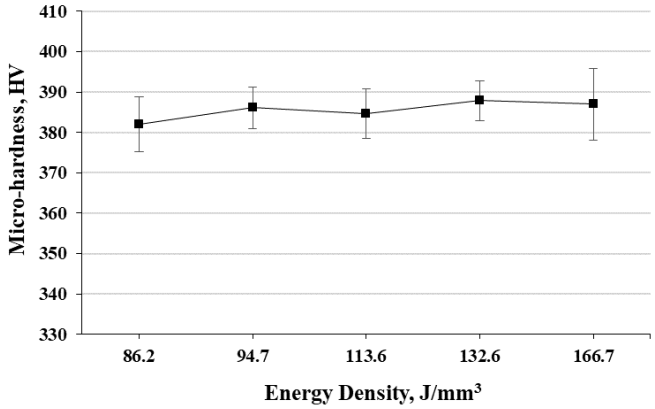

Fig 5. Micro-hardness results as a function of energy density.

3.4. Roughness measurements

In order to study the effect of the process parameters on the surface integrity of the selectively additive manufactured samples, surface profile measurements were carried out on the 3d-printed blocks. Fig 6 represented the surface roughness of the as-printed blocks as a function of energy density. The R_a parameter, which was commonly used to describe the general roughness of a selected surface, showed a slight modification on the blocks' surface by decreasing the energy density value. These average roughness (Ra) values were different from the average roughness value of 14.05 µm reported value by Nikiel et al [22] for the as-build Ti-6Al-4V grade 23 titanium powder. This could be due to the difference process parameters used for manufacturing the samples.

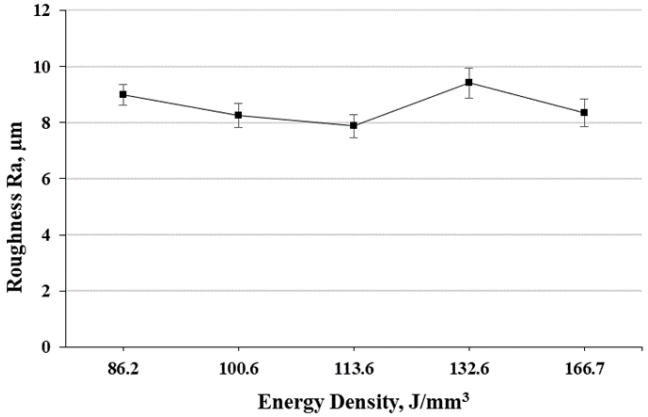

Fig 6. Surface roughness as a function of energy density.

4. **Conclusion**

In this work, the two most prominent metal 3d printing process parameters (laser power and scanning speed) of the powder bed fusion process were investigated to characterize the microstructure and surface integrity of the Ti6Al4V titanium alloy. The effect of different laser power and scanning speed on the microstructure, micro-hardness, and roughness were studied on the as-SLMed Ti6Al4V titanium samples.

The results showed that energy density primarily affects the size and ratio of the porosity, which are desirable for fabricating specimens with the additive manufacturing method. The results indicated that obtaining the microstructure with minor manufacturing defects in lower energy densities is more favorable. Also, the micro-hardness and surface roughness test results showed a slight reduction in the mechanical properties of the fabricated specimens by decreasing the energy density values from 166.7 to 86.2 J/mm^3.

Acknowledgments

Research conducted at the GIP-InSIC and LEM3 Laboratory, and financially supported by the "Institut Mines-Télécom: IMT" and GIP-InSIC. The authors would like to thank them for their technical/financial support in this research work.

References

[1] I. Gibson, D. Rosen, B. Stucker and M. Khorasani, "Design for additive manufacturing. In Additive manufacturing technologies," Springer, Cham, pp. 555-607, 2021.
[2] K. V. Wong and A. Hernandez, "A review of additive manufacturing," International scholarly research notices, 2012.
[3] S. L. Sing, A. Jia, Y. Y. Wai and F. E. Wiria, "Laser and electron-beam powder-bed additive manufacturing of metallic implants: A review on processes, materials and designs," Journal of Orthopaedic Research, vol. 34, no. 3, pp. 369-385, 2016.
[4] K. Al-Rubaie, S. Melotti, A. Rabelo, J. M. Paiva, M. A. Elbestawi and S. C. Veldhuis, "José M. Paiva, Mohamed A. Elbestawi, and Stephen C. Veldhuis. "Machinability of SLM-produced Ti6Al4V titanium alloy parts," Journal of Manufacturing Processes, vol. 57, pp. 768-786, 2020.
[5] M. Fischer, D. Joguet, G. Robin, L. Peltier and P. Laheurte, "In situ elaboration of a binary Ti–26Nb alloy by selective laser melting of elemental titanium and niobium mixed powders," Materials Science and Engineering: C, vol. 62, pp. 852-859, 2016.
[6] H. Ben Boubaker, P. Laheurte, G. Le Coz, S.S. Biriaie, P. Didier, P. Lohmuller, and A. Moufki, "Impact of the Loading Conditions and the Building Directions on the Mechanical Behavior of Biomedical β-Titanium Alloy Produced In Situ by Laser-Based Powder Bed Fusion, Materials, vol. 15, no. 2, pp. 509, 2022.
[7] H. Gong, D. Snelling, K. Kamran and A. Carrano, "Comparison of stainless steel 316L parts made by FDM-and SLM-based additive manufacturing processes," Jom, vol. 71, no. 3, pp. 880-885, 2019.
[8] N. Haghdadi, M. Laleh, M. Moyle and S. Primig, "Additive manufacturing of steels: a review of achievements and challenges," Journal of Materials Science, vol. 56, no. 1, pp. 64-107, 2021.
[9] L. Yang, K. V. Patel, K. Jarosz and T. Özel, "Surface integrity induced in machining additively fabricated nickel alloy Inconel 625," Procedia CIRP, vol. 87, pp. 351-354, 2020.
[10] S. Periane, A. Duchosal, S. Vaudreuil, H. Chibane, A. Morandeau, M. A. Xavior and R. Leroy, "Periane, S., Arnaud Duchosal, S. Vaudreuil, H. Chibane, Antoine Morandeau, M. Anthony Xavior, and R. Leroy. "Selection of machining condition on surface integrity of additive and conventional Inconel 718," Procedia CIRP, vol. 87, pp. 333-338, 2020.
[11] B. Dutta and F. S. Froes, "The additive manufacturing (AM) of titanium alloys," Metal powder report, vol. 72, no. 2, pp. 96-106, 2017.
[12] B. Poorganji, E. Ott,, R. Kelkar, A. Wessman and M. Jamshidinia, "Materials Ecosystem for Additive Manufacturing Powder Bed Fusion Processes," JOM, vol. 72, no. 1, pp. 561-576, 2020.
[13] M. K. Thompson, G. Moroni, T. Vanek, G. Fadel, R. I. Campbell, I. Gibson, A. Bernard, J. Schulz, P. Graf, B. Ahuja and F. Martina, "et al. "Design for Additive Manufacturing: Trends, opportunities, considerations, and constraints," CIRP annals, vol. 65, no. 2, pp. 737-760, 2016.
[14] H. Shipley, D. McDonnell, M. Culleton, R. Coull, R. Lupoi, G. O'Donnell and D. Trimble, "Optimisation of process parameters to address fundamental challenges during selective laser melting of Ti-6Al-4V: A review," International Journal of Machine Tools and Manufacture, vol. 128, pp. 1-20, 2018.
[15] A. Khorasani, I. Gibson, U. S. Awan and A. Ghaderi, "The effect of SLM process parameters on density, hardness, tensile strength and surface quality of Ti-6Al-4V," Additive manufacturing, vol. 25, pp. 176-186, 2019.

[16] G. Kasperovich, J. Haubrich, J. Gussone and G. Requena, "Correlation between porosity and processing parameters in TiAl6V4 produced by selective laser melting," Materials & Design, vol. 105, pp. 160-170, 2016.
[17] H. Gong, K. Rafi, T. Starr and B. Stucker, "The effects of processing parameters on defect regularity in Ti-6Al-4V parts fabricated by selective laser melting and electron beam melting," In 24th annual international solid freeform fabrication symposium—an additive manufacturing conference, Austin, TX, pp. 424-439, 2013.
[18] A. K. Singla, M. Banerjee, A. Sharma, J. Singh, A. Bansal, M. K. Gupta, N. Khanna, A. S. Shahi, and D. K. Goyal, " Selective laser melting of Ti6Al4V alloy: Process parameters, defects and post-treatments," Journal of Manufacturing Processes, vol. 64, pp. 161-187, 2021.
[19] O. Oyelola, P. Crawforth, R. M'Saoubi and A. T. T. Clare, "Machining of additively manufactured parts: implications for surface integrity," Procedia CIRP, vol. 45, pp. 119-122, 2016.
[20] E. Brinksmeier, G. Levy, D. Meyer and A. B. Spie, "Surface integrity of selective-laser-melted components," CIRP annals, vol. 59, no. 1, pp. 601-606, 2010.
[21] Y. Eyzat, M. Chemkhi, Q. Portella, J. Gardan, J. Remond and D. Retraint, "Characterization and mechanical properties of As-Built SLM Ti-6Al-4V subjected to surface mechanical post-treatment," Procedia CIRP, vol. 81, pp. 1225-1229, 2019.
[22] P. Nikiel, M. Wróbel, S. Szczepanik, M. Stępień, K. Wierzbanowski and A. Baczmański, "Microstructure and mechanical properties of Titanium grade 23 produced by selective laser melting," Archives of Civil and Mechanical Engineering, vol. 21, no. 4, pp. 1-16, 2021.
[23] M. Benedetti, E. Torresani, M. Leoni, V. Fontanari, M. Bandini, C. Pederzolli, and C. Potrich, "The effect of post-sintering treatments on the fatigue and biological behavior of Ti-6Al-4V ELI parts made by selective laser melting," Journal of the mechanical behavior of biomedical materials, vol. 71, pp. 295-306, 2017.